www.rericjournal.ait.ac.th

Thermochemical Energy Storage in Low Flow Liquid Desiccant Regenerator

Mustafa Jaradat*,[1]

Abstract – *Concentrated liquid desiccant (LD) presents an alternative means for energy storage for peak load shifting when appropriate supply for regeneration exists. The volumetric energy storage capacity is characterized by the stored energy per volume of the stored liquid desiccant. High flow liquid desiccant results in lower concentration spread of the solution and thus in lower storage capacity. In this paper, a liquid desiccant heat and mass exchangers was designed, built, and experimentally evaluated as a regenerator. The regenerator represents a low flow internally heated tube bundle. The main design-focus of the presented regenerator was to achieve improved heat and mass transfer coefficients, as well as higher chemical and thermal stability of the construction. The presented regenerator proved high thermal stability by high water temperatures up to about 90°C. A parametric analysis was performed to study the effect of varying desiccant flow rate, inlet air temperature, inlet desiccant temperature, and inlet heating water temperature on the water vapour desorption rate and the energy density. The experimental results showed a mass fraction spread in the range of 0.8 % to 5.7 % in the desiccant and a volumetric energy storage capacity of 17 to 117 kWh/m^3.*

Keywords – *energy storage, lithium chloride, liquid desiccant, regenerator, tube bundle.*

1. INTRODUCTION

Energy storage has become an important consideration in implementing solar energy for air dehumidification in air conditioning and drying applications. Time-dependent characteristic of solar radiation make storage necessary for continuous operations of air dehumidification using desiccant systems. Desiccants, either liquid or solid, represent an excellent mean for thermochemical heat storage through a reversible chemical reaction, adsorption or absorption process. The energy storage capacity of thermochemical storage is higher than the one of physical changes such as phase change or sensible heating [1]. However, there is a lack, in the literature, regarding energy storage and their effect on the performance of liquid desiccant air conditioning systems, [2]. Kabeel *et al.* [2] studied theoretically the effect of thermal and thermochemical energy storage on the performance of liquid desiccant air conditioning systems under different solar fractions. Also, he investigated the life cycle cost analysis for both types of energy storage modes.

Solid desiccants represent the majority of applied desiccants, and desiccant wheels are classified as the most applied type. Several experimental and numerical researches were conducted to investigate the performance of desiccant wheels for different materials and under different operating conditions, as in [3]-[6]. Zeolites and silica gels are the most common adsorbents as storage materials for thermochemical storage processes and water vapor is the adsorbate. Adsorption of water vapor in the adsorber discharges the stored energy and releases the stored heat to an air stream that in turn will be dehumidified and heated. For open cycle adsorption system with zeolite or silica gel as adsorbents, the water vapor can be adsorbed up to a total mass fraction of 30% to 40% of the storage material, Hauer [7]. With a charging temperature of 300°C, storage systems with zeolite as an adsorbent have a volumetric energy storage capacity density of up to 200 kWh/m^3, Hauer [8].

Hygroscopic salt solutions are the most common absorbents storage materials for absorptive thermochemical storage processes and water vapor is used as absorbate. The selection of the desiccant solution has great impact on the design and operation of the system. The sorbents need to be physically and chemically stable for numerous cycles. The desiccant must be able to hold significant weight fractions of water vapor at required partial pressures, ASHRAE Book of Fundamentals [9]. Several desiccant materials were reviewed and reported by several authors, [10]-[13]. Liquid desiccants are sorted into two main groups, glycols and hygroscopic salt solutions. The major unattractive characteristic of glycols is that they are extremely volatile. The existence of remarkably high concentration of glycol within the air stream is an indicator of elevated carryover of the desiccant solution when compared to desiccant salt solutions. This makes HVAC applications of glycols economically and environmentally unattainable in their existing state, [11]. Hygroscopic salt solutions are mixtures of any hygroscopic salt in water. Several hygroscopic salt solutions were studied and implemented in open cycle liquid desiccant systems. Halide salt water solutions such as calcium chloride ($CaCl_2$), lithium chloride (LiCl) and lithium bromide (LiBr) are the most widely used. $CaCl_2$ is the most affordable and attainable desiccant. However, its modest desiccation capacity, because of relatively higher vapor pressure, restricts its widespread

*Energy Engineering Department, German Jordanian University, Amman, Jordan.

[1]Corresponding author:
Tel: +962 6 4294444 Ext. 4221.
Email: Mustafa.Jaradat@gju.edu.jo.

implementation [12]. In contrast, LiCl is among the most stable liquid desiccants and it has significant dehydration mass fractions. Weak organic acid salts like potassium formate ($CHKO_2$) and sodium formate ($CHNaO_2$) are less corrosive than salt solutions as well as less volatile than glycols. Additionally, they are less viscous leading to less pumping power for circulation. In contrast, these types of salts possess low drying capacity unlike LiCl and $CaCl_2$ solutions. Furthermore, weak organic acids would be an appropriate environment for biological growth through the desiccant devices which may result in foul smells [13].

Liquid desiccant systems have several benefits compared to solid desiccant systems. They allow more design and installation arrangements compared to solid desiccant wheels in which dehumidification and regeneration takes place simultaneously in the same heat and mass exchanger. In contrary, in liquid desiccant systems the absorption and regeneration processes can be carried out off-site and they can be asynchronous, [14]. Concentrated liquid desiccants can be used as energy storage for peak load shifting when appropriate supply for regeneration exists, [15]. The capability to heat up the desiccant solution during the regeneration process lead to greater energy effectiveness than with solid desiccant types [16].

Liquid desiccant regenerators with packing material either in structured or random packing as the contact medium between air and solution are so far the most studied types of heat and mass exchangers. Related researches in packing liquid desiccant systems in both structured and random types of packed-bed type are reported by many authors, for example [17]–[20]. However, liquid desiccant flow rates need to be high in the packed beds to be able to provide good surface wetting of the packing materials and to maintain the desiccant solution at a relatively high temperature through the regeneration process [21].

Disadvantages of high desiccant flow rates are:

- Only a small concentration spread of the desiccant solution and therewith only small storage capacities can be reached,
- The risk of carryover of the desiccant droplets into the air stream which is generally larger for packed bed configurations compared to plate- or tube bundle heat and mass exchangers, and
- High auxiliary power consumption because of high pressure drop as a result of using mist eliminators.

Cheng and Zhang [22] reviewed the theoretical and experimental works on the regeneration methods of liquid desiccant applying solar thermal and solar electrodialysis regeneration methods. The results showed that electrodialysis regeneration system is more energy-efficient compared to solar thermal regeneration system, however it is more expensive.

Modeling of packed towers liquid desiccant systems have been investigated by many authors. Distinct additions in this area were performed by Naik *et al.* [23]-[25] for different air to desiccant solution flow-configurations. The performance of a counter-flow adiabatic dehumidifier was simulated using a finite difference model using correlations between the heat and mass transfer coefficients from one side and the thermal and moisture removal effectiveness, respectively, [23]. Also, Naik *et al.* [24] developed a simplified thermodynamic approach to analyze the dehumidifier/regenerator performance in a cross flow configuration. Furthermore, the performance of adiabatic dehumidifier/regenerator in a counter flow configuration was predicted by applying a two-dimensional model. The influence of the air humidity ratio on the liquid desiccant dehumidifier/regenerator was studied experimentally for the validation of the model, [25]. The benefits of low flow liquid desiccant systems were discussed by Lowenstein *et al.* [16], [21]. Further investigations of low flow systems for increasing energy storage capacity were performed by the Bavarian Center for Applied Energy Research (ZAE Bayern) [7], [8], [15], and [26]. Field test investigations of a low flow liquid desiccant system for air conditioning applications with ambient air conditions were previously studied by several authors, such as Gommed and Grossman [27], Abdel-Salam *et al.* [28], and Jaradat *et al.* [29]. An energy storage density of 150 kWh/m^3 has been reached in a low-flow LDCS with an aqueous LiCl solution developed by ZAE Bayern. Driven by district heating, it provides 12 kW of cooling to a jazz club in Munich [8]. A similar but solar driven LDCS manufactured by L-DCS Technology operating in Singapore that provides 100 kW of cooling and dehumidification achieved an energy storage density of 185 kWh/m^3 [26].

However, low flow liquid desiccant systems require continuous cooling in the absorber and continuous heating in the regenerator. The area where the desiccant solution and the air flow come together is amongst the essential factors for the entire system performance and it affects the energy consumption of the system. According to the operating conditions, the components coming in contact with the salt solution need to resist corrosion and also to have specific ranges of thermal conductivity and coefficient of thermal expansion. Polymers such as polypropylene and polycarbonate are resistant to corrosion. However, the thermal expansion of polymers affects the stability of the construction and their thermal conductivity is low, in the range of 0.2 W/mK for polypropylene and polycarbonate [30].

Heat and mass exchangers made of polymers were tested in regeneration mode. Keßling *et al.* [15] presented an internally cooled/heated absorber/regenerator liquid desiccant heat and mass exchanger made of polypropylene. Also, Mesquita [31] tested experimentally a single channel internally cooled absorber made of polycarbonate. However, when those components were examined for the regeneration process, it was observed that the polymer plates did not have sufficient clearance for thermal expansion, which caused them to deform. Thus, the regeneration of the diluted solution was conducted by heating the solution externally.

As an alternative to polymer materials, metals which have a much lower thermal expansion have been suggested. Commercially available plastic-coated

aluminum plates have been used as a desiccant absorber, Lowenstein [11]. However, it was observed that the plastic coatings failed to properly protect the aluminum plates, and several plates were severely corroded by the desiccant solution.

Yamaguchi *et al.* [32] studied experimentally an integrated liquid desiccant vapor compression system. The absorber was integrated to the evaporator coils and the regenerator was integrated to the condenser coils. The outer surface of coils and fins were uniformly coated to prevent corrosion due to the presence of the LiCl solution. However, high flooding rate were used in which the desiccant to air mass ratio was in the range of 2.0. Moreover, the desiccant solution was sprayed over the coils and fins and no study of carryover or the use of mist eliminators was reported.

Plate-type heat and mass exchangers lend larger surface area than tube-types taking up similar space. However, tube-type has the advantage of uniform distribution of heating water inside the serpentine tubes compared to the internal passages of typical twin-wall plate type. Also, tube-type can support higher operating temperatures and pressures than plate-type heat and mass exchangers.

According to the operating conditions, the components that come in contact with the salt solution need to resist corrosion and also have a specific range of thermal conductivities and coefficients of thermal expansion. Polymers such as polypropylene and polycarbonate are resistant to corrosion. However, the thermal expansion of polymers affects the stability of the construction. When thermal gradients are present this can lead to stresses in the component. Plate-type heat and mass exchangers were tested as an internally heated regenerator. The plates were made of polymers (polycarbonate/polypropylene) with a coefficient of linear thermal expansion in the range of $\alpha = 6.5 \times 10^{-5}\ K^{-1}$. It was noted that the plates exhibited some expansion with a heating-water temperature of about 60°C [15], [31].

This paper presents a novel internally heated bundle-type regenerator made of copper. The copper tube-bundle is protected from corrosion with a thin layer of powder coating. Furthermore, textiles are attached to the tubes to reduce the velocity of the sorbent and to enhance wetting of the surface. The novel regenerator is described in section 2 of this paper. Section 3 presents the sizing of the tube bundle. Section 4 presents the experimental set-up in the laboratory. High standard instrumentation was supplied, namely for the measurements of air flow rates (vortex sensors), solution flow rate (magnetic inductive flow meters), density sensors to evaluate sorbent concentrations, and humidity sensors for air. Section 5 presents the test matrices and methodology. Finally, section 6 presents experimental results of the regeneration process for the controlled variables of the circulated fluids on the energy storage capacity.

2. DESCRIPTION OF THE INVESTIGATED REGENERATOR

In the presented study, an internally heated, desiccant based tube-bundle regenerator with an effective surface area of 4.2 m^2 was experimentally examined for the regeneration of the diluted solution.

The design of the components utilizes novel components and ideas in order to enhance the main regenerator components; the air to desiccant contact surface, liquid desiccant distributor, and water distribution. The main goal of the current research is to enhance the heat and mass transfer within the non-adiabatic absorber and regenerator by improving the water to desiccant contact surface. Furthermore, this work is aimed at improving the contact surface between the air and the desiccant solution. Prior to the presented study, various wicking performances of different fabrics were evaluated experimentally. Textiles with different compositions, thicknesses, and surface densities were tested at various desiccant solution mass fractions. The absorption capacity and diffusion behaviour were evaluated. Moreover, a liquid desiccant distribution device was designed to facilitate a uniform distribution of the liquid desiccant at low flow rates, as possible, over the exposed surface. Various distribution pipe designs were investigated, as well. Improving the air-desiccant solution interface can possibly eliminate entrainment of the desiccant solution into the process airstream (carryover).

The regenerator consists of 22 tubes made of copper. The tubes are 5 m long, have an outer diameter of 12 mm and a wall thickness of 1 mm. The copper tubes were coated with a thin powder layer with a thickness of 0.24 mm to protect them from the corrosive LiCl solution. Figure 1 shows the coated copper tubes.

Fig. 1. Powder-coated copper tubes.

The coated tubes were covered with 0.4 mm thick sleeves made of cellulose. Figure 2 shows the tubes after being covered with the textile sleeves.

The case of the regenerator was made of 10 mm-thick polycarbonate. The tube bundle is held in the polycarbonate housing with pressure clamps and is soldered together with an offset of 20 mm. The connections of the tube bundle were located outside the regenerator housing. Every second tube was connected in series. Figure 3 shows a 3D assembly of the tube-bundle regenerator.

The liquid desiccant distributor consists of 23 parallel polymer pipes to horizontally distribute the desiccant over the textile attached to the copper tubes. The parallel pipes extend outwardly from openings in the liquid desiccant manifold and are closed from the free end. Each pipe is perforated from both sides, the double-sided holes allowing the simultaneous wetting of two tube rows as shown in Figure 4. The diameter of the discharge holes is 0.5 mm and the liquid desiccant is distributed horizontally at the center of each copper pipe, as shown in Figure 5.

Fig. 2. Powder coated copper tubes covered with textile.

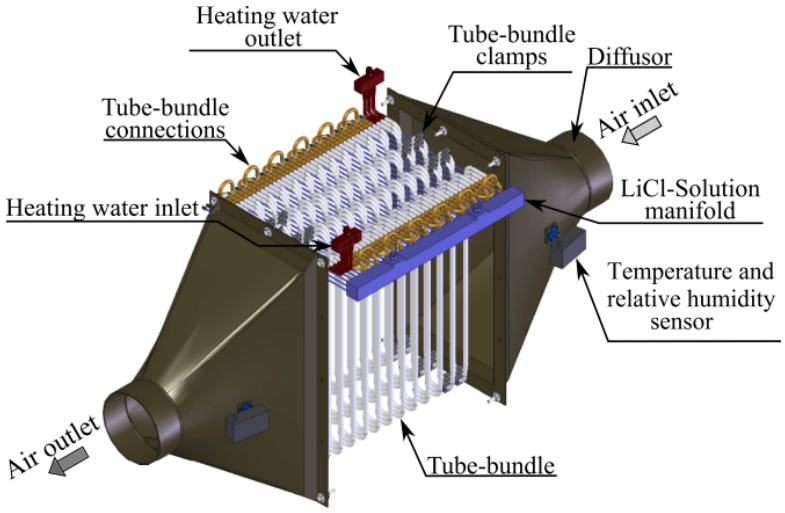

Fig. 3. A **3D assembly of the regenerator along with the illustration of heating water and desiccant manifolds.**

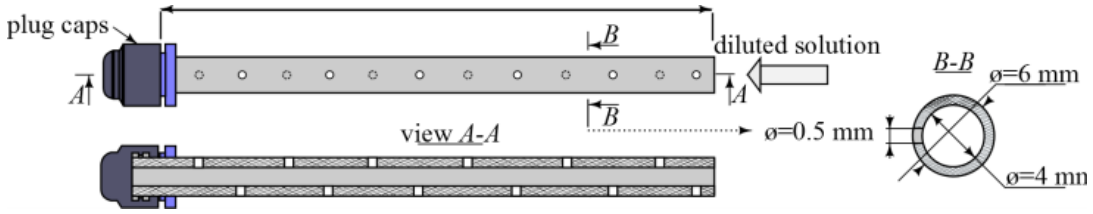

Fig. 4. Perforated pipe of the liquid desiccant distributor in the tube-bundle heat and mass exchanger.

In the present study, the solution flow rate was set in the range between 10 to 80 kg/h which represent an air to solution mass ratio $r_m = 40\ to\ 5\ kg_a/kg_{sol}$ in the present study. The selection of this flow rate was based on two criteria. Firstly, it was chosen by referring to the literature regarding the definition of low flow liquid

desiccant systems. In the literature, there is no specific definition of r_m , however, some ranges have been mentioned such as 10 to 50 kg/kg [11] and up to 150 for "micro-flow" liquid desiccant systems [15]. So the target of this study was to investigate a wide range of solution flow rates. Secondly, it was chosen based on experimental evaluation of the liquid desiccant distribution system. In the presented regenerator, the liquid desiccant is distributed via a number of perforated Plexiglas pipes that penetrate the tubes, as shown in Figure 5, to distribute the desiccant solution horizontally over the textiles attached over the exchange surfaces.

Fig. 5. Perforated desiccant pipes penetrating the tube-bundle.

Fig. 6. Bending of a copper tube using hand bending machine.

The solution flow rate of 10 to 80 kg/h represents the marginal flow rates that ensure the minimal maldistribution of the solution through the perforated pipes over the textile by optimizing the perforation diameter as a function of the position of each perforation from the desiccant manifold box.

3. SIZING OF THE TUBE-BUNDLE

Sizing of the tube bundle heat and mass exchangers was done based on the required surface area for heat and mass transfer, *i.e.* the tubes diameter, length, and arrangement.

In the planning phase, the aim was to construct the tube bundle in the laboratory. Therefore, the geometry of the tube bundle was, to some extent, determined according to the laboratory equipment for self-assembly (bending profile of the hand bending machine for copper pipes). The pipe diameter was determined according to the available copper types (soft, hard, and half-hard copper) considering the ability of bending and the stability in the construction stage (hard copper can't be bended and soft copper is easy to bend but not stable). The tube bundle heat and mass exchanger was constructed of half-hard copper tubes. Each copper tube is 5 m long, 12 mm outer diameter and 1 mm wall thickness. The bending of the tube bundle was done with hand bending machine with a bending radius of about 20 mm as shown in Figure 6. Furthermore, to ensure that the tubes are not kinked during the bending process the copper tubes were filled with sand prior to the bending operation. The pressed sand prevents kinking of the tubes during bending.

Every second tube was connected in series, as shown in Figure 7. This prototype consists of 22 tubes staggered with two offsets. The tubes were soldered together with an offset of 20 mm. the distance between

two adjacent tubes in the air flow direction was set to 6mm which represents the outer diameter of the desiccant distributor perforated pipe.

The tubes arrangement is shown in Figure 8, two rows of tubes are offset from each other. The distance between the tubes of the first and second row S_2 (transverse pitch) is equal to 19.4 mm ($2r_{tube,o} + d_{plexiglas}$). The distance S_1 (longitude pitch) corresponds to the mean diameter of the bending profile of about 40 mm.

Fig. 7. Solder joints and the pipe connectors.

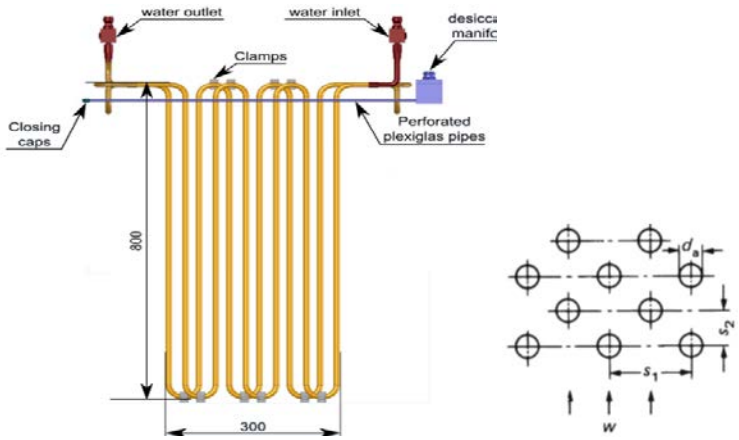

Fig. 8. Arrangement of the tubes in the tube-bundle (left), and staggered tubes illustration [33].

The arrangement factor, $f_{A,stag}$, with staggered pipe arrangement is calculated as:

$$f_{A,stag} = 1 + \frac{2}{3b} \quad (1)$$

The determination of the void fraction, ψ , according to the pipe arrangement is given by:

$$\psi = 1 - \frac{\pi}{4a} \quad \text{for } b \geq 1 \quad (2)$$

where, $a = \frac{S_1}{d_o}$ and $b = \frac{S_2}{d_o}$ represent the crosswise and stream-wise pitch-to-diameter ratios, respectively.

The radiation and the conduction heat transfer components through the desiccant film are neglected. The convective heat transfer from the heating-water to the airstream through the pipe is given as:

$$\dot{Q} = U\, A\, \Delta T_{log} = \dot{m}_{hw} c_{p,hw} \left(T_{hw,i} - T_{hw,o}\right) \quad (3)$$

U is the overall heat transfer coefficient; A is the total surface area ($A = \pi\, N\, d_o\, l$) ; ΔT_{log} is the log mean temperature and is calculated as follows:

$$\Delta T_{log} = \frac{\Delta T_2 - \Delta T_1}{\ln\left(\frac{\Delta T_2}{\Delta T_1}\right)} \quad (4)$$

The determination of the UA value in W/K for the cylindrical surface (tube) is calculated as:

$$UA = \frac{1}{\frac{1}{\alpha_o\, \pi\, d_o\, l} + \sum \frac{\ln\left(r_{i+1}/r_i\right)}{2\pi\, \lambda\, l} + \frac{1}{\alpha_i\, \pi\, d_i\, l}} \quad (5)$$

where, λ is the thermal conductivity of the tube in $W/m\,K$; d_i and d_o are the tube inner and outer diameter in m; α_i and α_o are the internal and external heat transfer coefficients in W/m^2K ; r_i is the inner tube radius in m; l is the tube length in m.

The external and internal heat transfer coefficients were calculated using Nusselt number with fully

developed turbulent flow according to VDI Heat Atlas [33].

The total surface area of the tube bundle was found to be equal to 5.8 m^2 and thus the total length of the tubes is calculated as:

$$L_{tube-bundle} = \frac{A_{tube-bundle}}{\pi d_{o,textile}} = \frac{4.8\ m^2}{3.14 \times\ 0.0134 m} \cong 114\ m$$

The number of tube-rows from the tube bundle is thus 22.8, since each tube is 5 m long. And thus, the dimensions internal dimensions of the tube bundle were 300 mm × 800 mm × 432 mm (width × height × length).

4. EXPERIMENTAL SETUP AND INSTRUMENTATION

4.1 Experimental Setup

Air, desiccant solution, and heating water handling units were installed to control the required conditions for the circulated fluids (air, desiccant solution, and heating water) for the regeneration experiments. The handling units emulate predefined boundary conditions (flow rates, temperatures, and mass fractions) in order to study the dynamic behavior of the regeneration process. According to the required conditions, airstream could be cooled, heated, de/humidified through the air handling unit. The air handling unit consists of an air cooler with a capacity of 16.8 kW, two air-heaters with a heating capacity of 38 kW, air-humidifier steam generator with a capacity of 30 kg/h, two fans, air filters, and air dampers.

The internal heat for the regenerator is handled by a water conditioning unit. The hydraulic module is equipped with one diaphragm expansion vessel and a proportional–integral–derivative controller-electrical heater with a heating capacity of 18 kW.

The desiccant solution handling unit consists of two plastic tanks for the diluted and the concentrated desiccant solution, diaphragm pumps, filters, and a powder-coated copper coil immersed in the diluted-solution tank and connected to one of the water handling units. Figure 9 shows an overall view of the regenerator with air, water and desiccant handling units.

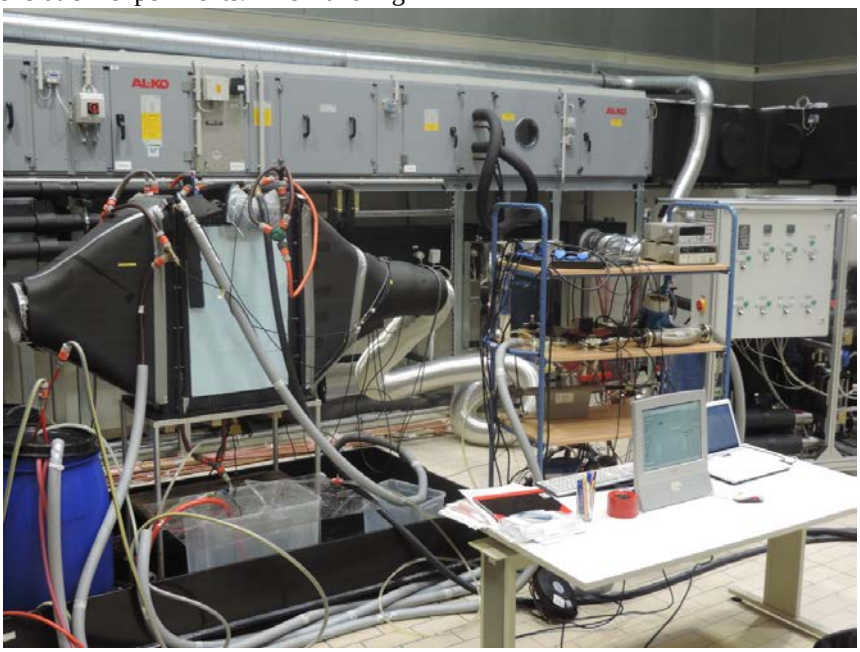

Fig. 9. Liquid desiccant regenerator in the pilot plant stage.

4.2 Instrumentation

The air flow rate was measured using ultrasonic and ultrasonic-vortex flow-meters connected in series. The air flow rate was measured with an ultrasonic flow meter (Prosonic Flow B 200) with an accuracy of 1.5% of the logged signal. The second sensor uses the principle of vortex integrated with ultrasonic, for the measurement of the vortex shedding with an accuracy of 1% of the measured value.

Air relative humidity and temperature were continually monitored by using humidity and temperature sensors (testo 6610) with an accuracy of ± 1% of relative humidity and ± 0.3 K for temperature readings. Two temperature and relative humidity sensors were applied in the middle of the round-to-rectangle ducts (at the inlet and outlet) and they were positioned in the center of the air flow streams.

The internal heat of the regenerator and the regulation of the temperature of the solution were controlled by a water handling unit. Water flow rate was in-line monitored using a magnetic inductive flow meter (OPTIFLUX 1050) with an accuracy of 0.5% of the measured value. In addition, the inlet and outlet temperatures were inline monitored using Pt100 sensors with an uncertainty of ± 0.5 K.

The desiccant circuit consists of two desiccant storage tanks made of Polyethylene. The desiccant solution is drawn from the primary tank with a membrane pump. A filter with a pore size of 300 μm is installed at the inlet in order to prevent clogging of the discharge-bores in the liquid desiccant distribution

system from possible contaminants. A heat exchanger with an exposed surface area of 1.2 m^2, made of powder coated copper coil, is immersed in the primary solution tank to regulate the temperature of the solution according to the required conditions.

The temperature of the solution at inlet and outlet, the solution flow rate at the inlet, and the density of the solution at the exchanger inlet were continually monitored. Furthermore, the density of the solution and the accompanied temperature were measured by taking samples of the solution at the outlet and from the desiccant storage tank. The desiccant mass flow rate was monitored using a coriolis flow-meter (Promass 80108) with an accuracy of 0.15% of the measured value. The density and the temperature of the LiCl solution discharged from the primary tank to the heat and mass exchanger was continually monitored while passing through a density meter. The density transmitter used in the desiccant circuit was an L-Dens 323 sensor with an accuracy of 0.001 g/cm^3. Figure 10 shows the experimental setup of the circulated fluids.

The signals from the instruments were sent to a data acquisition module. The data were internally averaged over a 10 seconds period.

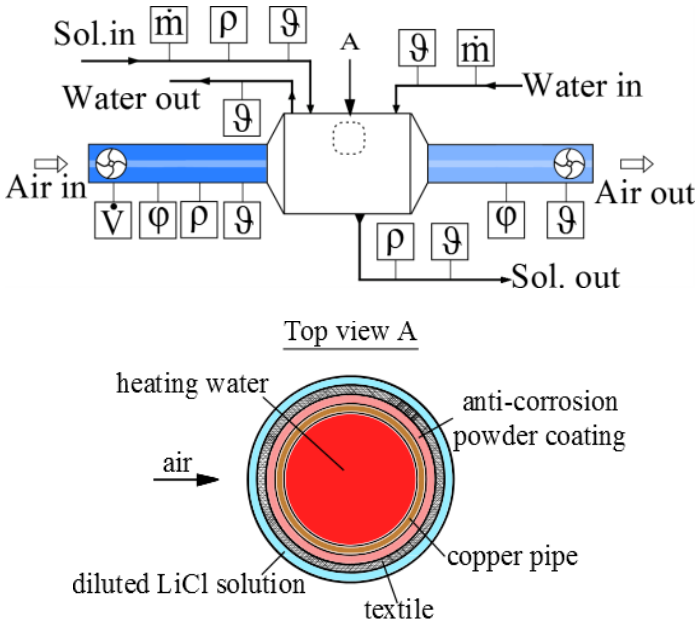

Fig. 10. The experimental setup of the circulated fluids, with a cross section of the tube-bundle regenerator.

Table 1. Test matrix (input values) for the internally heated tube-bundle regenerator.

	$\dot{m}_{sol}$ kg/h	ϑ_a °C	ϑ_{sol} °C	ϑ_{hw} °C	r_m
TS1	11-83	40.5	38.2	70.3	34-4.5
TS2	40.1	28-50	38.2	70.4	10
TS3	40.5	40.4	25-50	70.2	10
TS4	40.4	40.6	38.1	50-89	10

5. METHODOLOGY

The regenerator was tested under internally-heated conditions by using heating water stream. In total, 16 experiments were performed in four test sequences (TS) by varying one of the inlet parameters while keeping the other parameters fixed. The controlled inlet parameters for the parametric analysis, shaded gray, are listed in Table 1.

In the test sequences 1 to 4, one of the following inlet parameters; the desiccant solution flow rate $\dot{m}_{sol}$, the air temperature ϑ_a , the desiccant solution temperature ϑ_{sol}, and the heating-water inlet temperature ϑ_{hw} were varied, respectively. During these experiments all remaining parameters were kept (nearly) constant, as shown in Table 1. The aim of the experiments was to study the effect of the mentioned controllable parameters on the energy storage capacity.

The water vapour desorption rate from the LiCl-H_2O diluted solution to the scavenging air stream solution in the regeneration process, $\dot{m}_v$, was calculated regarding the solution side (SS). On the solution side, it is a function of the water content spread of the desiccant $\Delta X = X_{dil} - X_{con}$, as given in Equation 6.

$$\dot{m}_{v,SS} = \dot{m}_{LiCl}(X_{dil} - X_{con}) \quad (6)$$

Where, X is the mass of water per the mass of LiCl (in kg_{H2O}/kg_{LiCl}). It is given in Equation 7.

$$X = \frac{1-\xi}{\xi} \quad (7)$$

The LiCl-H_2O solution mass fraction, ξ_{sol}, is the ratio of the mass of the dissolved salt, m_{LiCl}, to the mass of the solution, m_{sol},, which consists of the mass of the

solvent (water), m_w,, and the mass of solute (LiCl salt) as given by Equation 8, Keßling *et al.* [15]:

$$\xi_{sol} = \frac{m_{LiCl}}{m_{LiCl} + m_w} = \frac{m_{LiCl}}{m_{sol}} \quad (8)$$

Applying Equations 7 and 8 in Equation 6, the desorbed water vapor is equal to:

$$m_v = m_{LiCl}\left(\frac{1-\xi_{dil,sol}}{\xi_{dil,sol}} - \frac{1-\xi_{con,sol}}{\xi_{con,sol}}\right) \quad (9)$$

Open liquid-sorption system is a cycle with two processes; the absorption and the regeneration processes. The dehumidification process is driven only by concentrated desiccant solution without further thermal energy supply. The concentrated solution can serve as storage medium for the driving energy for the dehumidification process. Comparable to thermal storage systems that can be evaluated by the temperature difference between inlet and outlet for the stored thermal energy, in liquid desiccant systems the concentration difference between concentrated and diluted solution is a measure for the stored energy. The higher the concentration difference is, the higher is the amount of stored energy. Storing energy by means of a concentration difference belongs to the thermochemical storage.

The volumetric energy storage capacity quantifies the stored energy per volume of the storage medium. The absorption of water vapor by the concentrated LiCl solution causes a release of heat (stored in a thermochemical form in the concentrated solution). This is equal to the sum of the enthalpy of condensation ($\dot{m}_v\, h_{fg}$) and the enthalpy of mixing ($\dot{m}_v\, h_{dil}$).The total enthalpy of sorption during the absorption process is given by Equation 10:

$$\dot{H}_{lat} = \dot{m}_v \left(h_{fg} + h_{dil}\right) \quad (10)$$

and thus, the volumetric storage capacity is in Equation 11 (31):

$$C_s = \frac{H_{lat}}{V_{dil,sol}} \quad (11)$$

Where, the volume of the diluted solution is given by Equation:

$$V_{dil,sol} = \frac{m_{dil,sol}}{\rho_{dil,sol}} \quad (12)$$

The expression for volumetric energy storage capacity of a liquid desiccant system is thus given as:

$$C_s = \rho_{dil,sol}\xi_{dil.sol}\left(\frac{1-\xi_{dil,sol}}{\xi_{dil,sol}} - \frac{1-\xi_{con,sol}}{\xi_{con,sol}}\right)h_{fg} = \rho_{dil,sol}\xi_{dil.sol}\Delta X h_{fg} \quad (13)$$

Thus, the concentrations of the diluted and the concentrated solution and the density of the diluted solution allow an assessment of the energy storage potential of the system.

The determination of the concentration ξ_{sol} of an aqueous LiCl solution before and after the sorption process can be iteratively determined as a function of the solution density (ρ_{sol}) by applying the equations given by Conde [34].

6. RESULTS AND DISCUSSION

In the following, results of 16 regeneration measurements are presented. Each of the experimental results is derived from nearly stationary conditions after a start-up time of about 60 to 90 min. The effect of the controlled variables on the water vapour desorption rate from the diluted LiCl-H_2O solution, the concentration spread, and the volumetric energy capacity for each controlled variable.

6.1 Desiccant Solution Flow Rate

Table 2 shows the inlet parameters for the experiments carried out in the internally heated tube bundle regenerator with the solution mass flow rate as a controlled variable. In the first test sequence, five experiments were conducted in which the solution flow rate is varied in the range between 11 kg/h and 83 kg/h. The range of flow rates represents an air to solution mass ratio range between 34 and 5 kg/kg.

In the performed experiments, the air stream, the diluted solution, and the heating-water inlet temperatures were held fixed at about 40°C, 38.5°C, and 70°C, respectively. As shown in Table 2, it was very difficult to hold the air inlet humidity ratio fixed since the experiments were performed at different days. The other inlet parameters were kept, nearly, constant for all experiments. Figures 11 and 12 show the effect of varying the desiccant flow rate on the regenerator performance.

Table 2. Inlet parameters with desiccant solution flow rate as a controlled variable.

	$\dot{m}_{sol}$ kg/h	$\dot{m}_{hw}$ kg/h	ϑ_a °C	ω_a g/kg	ϑ_{sol} °C	ϑ_{hw} °C
I	11.1	408.0	40.8	9.4	38.6	69.7
II	21.9	415.6	40.2	10.4	38.5	70.4
III	39.8	405.7	40.6	9.2	38.8	70.5
IV	59.5	405.9	40.5	8.5	38.0	70.4
V	82.6	404.7	40.4	11.2	37.0	70.4

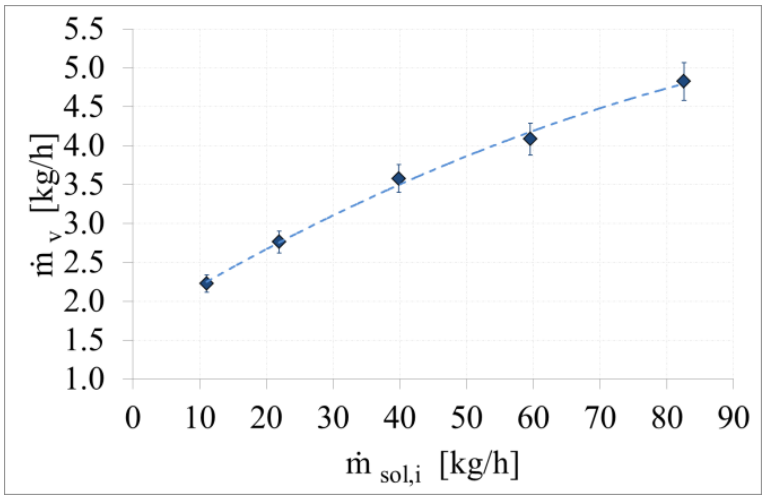

Fig. 11. The effect of desiccant mass flow rate on the water vapour desorption rate.

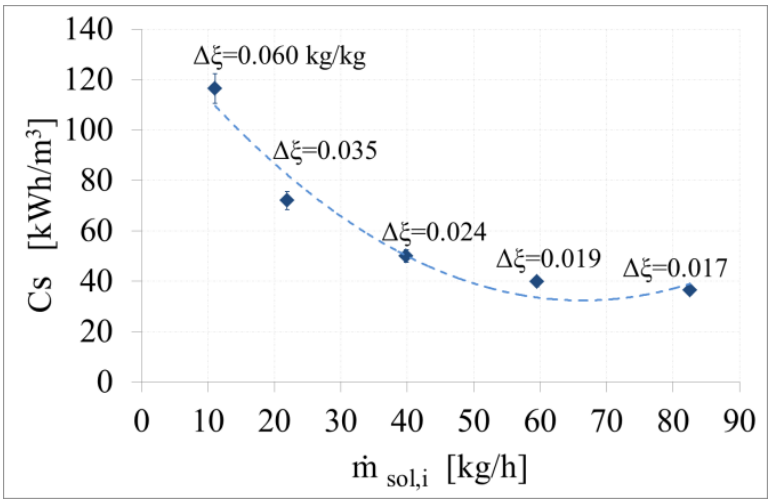

Fig. 12. Change in solution mass fraction and storage capacity as a function of desiccant mass flow rate.

Figure 11 shows the effect of increasing the desiccant solution mass flow rate on the water removed from the diluted desiccant solution. The water vapour desorption rate increases remarkably with increasing desiccant flow rate, as long as the air flow rate provided is sufficient and the outlet air is not saturated. This trend of the values in the diagrams is expected as that the vapor pressure within the solution increases for lower mass fractions as well, it raises by increasing the solution temperature. As a result, heated and diluted solutions offer the best regeneration. Also, increasing the solution flow rate is accompanied with a reduction in the concentration spread (Δξ), as shown in Figure 12, and thus increases the mass transfer potential from the solution to the air stream. Furthermore, the wetting of the textile-sleeves attached to the tubes is increased by increasing the solution flow rate, and thus enhances the heat and mass transfer.

The concentration spread is reduced, as expected, by increasing the desiccant flow rate, as shown in Figure 12. An increase in the solution concentration of 6% is achieved for a solution flow rate of 11 kg/h (air to solution mass ratio of 34) compared to an increase of 1.7% for a solution flow rate of 82 kg/h (air to solution mass ratio of 4.5). The variation in the concentration spread is decreased by increasing the solution flow rate, the variation in the solution concentration is only 9.7 % between the fourth and the fifth experiments.

Also, the volumetric energy capacity increases significantly by decreasing the solution flow rate as shown in Figure 12. An energy density of 116 kWh/m^3 was achieved for air to desiccant mass ratio $r_m = 34$ with a charging temperature of 70°C.

6.2 Air Inlet Temperature

Table 3 presents the inlet parameters of the internally heated tube-bundle regenerator with the air inlet temperature as a controlled variable. The second test sequence consists of three experiments in which the air inlet temperature was varied by extra heating the air entering the regenerator in the range between 28°C and 50°C.

The effect of air inlet temperature on the performance of the regenerator is shown in Figures 13 and 14.

As shown, the water vapour desorption rate as well as the change in solution mass fraction is affected slightly by varying the air inlet temperature. This effect is fairly weak since the preheated desiccant solution has higher thermal capacity compared to the air stream. Also, the desiccant film is continuously heated by the heating-water stream with a temperature of 70°C.

Table 3. Inlet parameters with air inlet temperature as a controlled variable.

	$\dot{m}_{sol}$ kg/h	$\dot{m}_{hw}$ kg/h	ϑ_a °C	ω_a g/kg	ϑ_{sol} °C	ϑ_{hw} °C
I	44.2	412.6	28.0	9.7	37.4	70.2
II	41.8	405.7	40.6	9.2	38.8	70.5
III	40.1	413.5	49.8	10.8	38.4	70.3

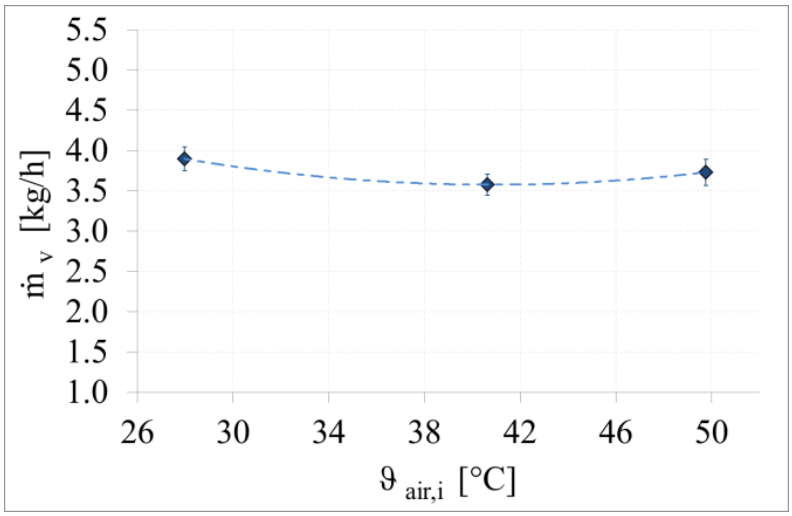

Fig. 13. Water vapour desorption rate as a function of air inlet temperature.

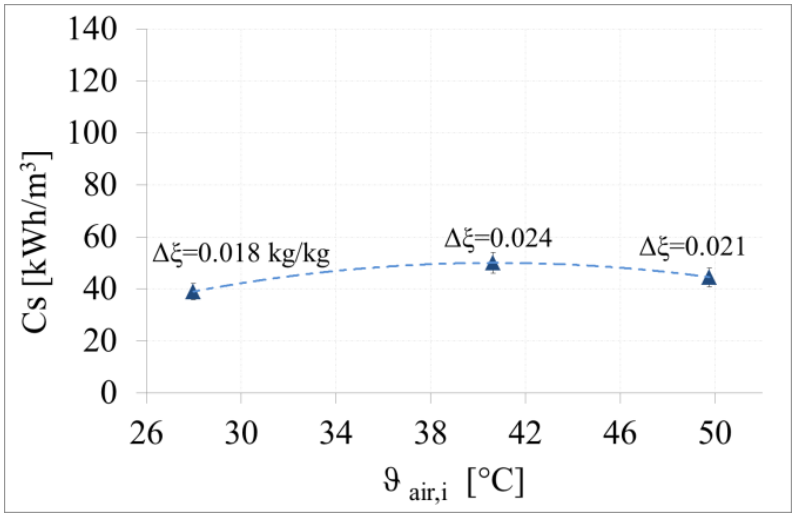

Fig. 14. Change in solution mass fraction and storage capacity as a function of air inlet temperature.

Table 4. Inlet parameters with desiccant solution inlet temperature as a controlled variable.

	$\dot{m}_{sol}$ kg/h	$\dot{m}_{hw}$ kg/h	ϑ_a °C	ω_a g/kg	ϑ_{sol} °C	ϑ_{hw} °C
I	39.9	413.1	40.1	9.7	25.6	70.3
II	41.6	414.4	40.9	9.8	31.2	69.5
III	39.8	406.7	40.6	9.2	38.8	70.5
IV	40.6	408.4	40.0	9.9	47.6	70.3

6.3 Desiccant Solution Inlet Temperature

Table 4 presents the inlet parameters of the conducted experiments through the internally heated tube-bundle regenerator with the desiccant solution inlet temperature as a controlled variable. In total, 4 experiments were carried out by varying the solution inlet temperature at four values range between 26°C to 48°C.

The water vapour desorption rate, the solution outlet concentration, and the energy density are increased by increasing the inlet solution temperature, for the given conditions, as shown in Figures 15 and 16.

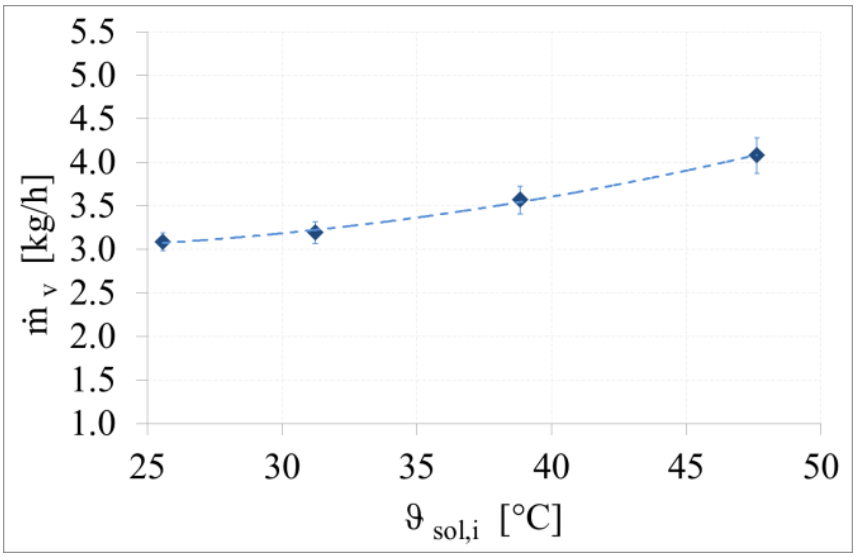

Fig. 15. Water vapour desorption rate as a function of desiccant solution inlet temperature.

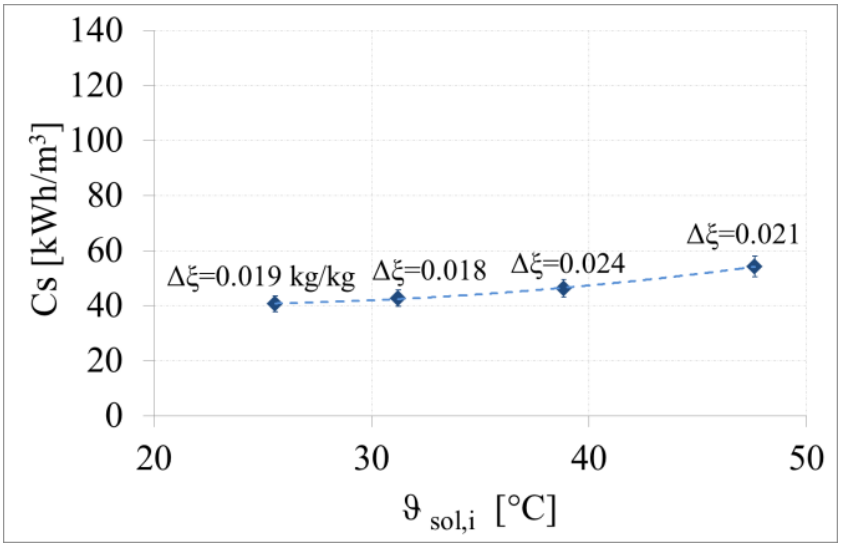

Fig. 16. Change in solution mass fraction and storage capacity as a function of desiccant temperature.

The water vapour desorption rate is increased by increasing the solution inlet temperature. The water vapour desorption rate was in the range of 3.1 and 4.1 kg/h. The increase in water vapour desorption rate, by increasing the solution temperature from 25.6 to 47.6 °C, is relatively small taking in the account that the regenerator is internally heated with heated water of 70 °C.

6.4 Heating Water Inlet Temperature

Table 5 presents the inlet parameters of the internally heated tube-bundle regenerator with the heating-water inlet temperature as a controlled variable. The heating water inlet temperature is increased at four different temperatures in the range of 50 to 89°C. As seen in Table 5, there is some deviation in the air humidity ratio at the regenerator inlet than the desired one (here 10 g/kg) in the range of ±1.3 g/kg. A possible explanation is that this variation is a consequence of the inherent variability in the ambient air conditions delivered to the air handling unit. The air conditions vary during the course of the day also some of the experiments (for the same controlled variable) were performed on different days. This variation is clearly observed between the 3rd and 4th test sequences.

Table 5. Inlet parameters with heating water inlet temperature as a controlled variable.

	$\dot{m}_{sol}$ kg/h	$\dot{m}_{hw}$ kg/h	ϑ_a °C	ω_a g/kg	ϑ_{sol} °C	ϑ_{hw} °C
I	40.4	415.9	40.5	10.2	36.5	50.4
II	39.8	406.7	40.6	9.2	38.8	70.5
III	40.2	413.7	40.6	11.3	38.8	79.8
IV	41.3	408.4	40.7	8.9	38.3	89.2

The increase in the heating-water inlet temperature is accompanied with a significant increase in the air inlet temperature and humidity ratio up to 28.1 K and 13.6 g/kg, respectively. The effect of increasing the heating-water inlet temperature on the water vapour desorption rate from the diluted solution, the increment of the solution mass fraction and the energy storage are shown in Figures 17 and 18.

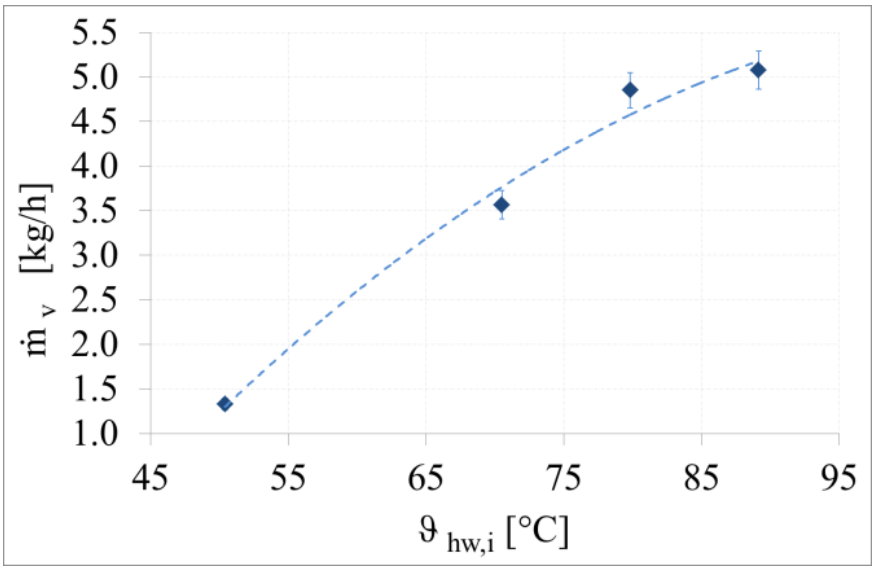

Fig. 17. Water vapour desorption rate as a function of the heating-water inlet temperature.

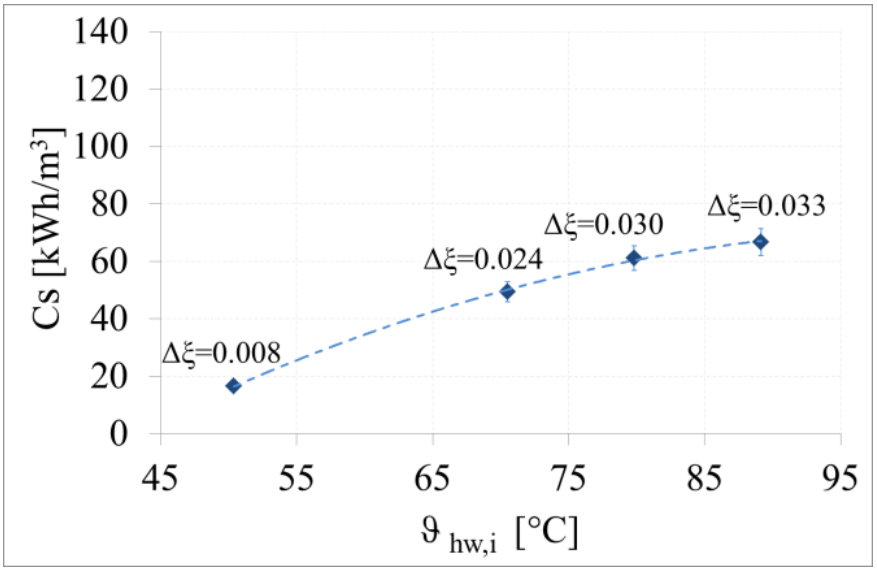

Fig. 18. Change in solution mass fraction and storage capacity as a function of heating-water inlet temperature.

As shown, the water vapour desorption rate as well as the outlet desiccant mass fraction increases by increasing the heating water inlet temperature. Heat drives the regeneration process in open sorption systems and this water vapor directly evaporates into ambient air. The water vapor desorption rate increases by increasing the heating water temperature. Increasing the water temperature will cause an increase in the vapour pressure of the desiccant solution and thus will increase the removed moisture from the desiccant solution into the scavenging airstream. A water vapour desorption rate of about 1.3 kg/h is observed for a heating water inlet temperature of 50°C accompanied with a concentration spread of about 1%. This increase in the desiccant solution mass fraction is considered as a good achievement for a heating water temperature of 50°C, compared to packing systems. Moreover, a heating water temperature of 75°C could be considered as an optimal temperature with a concentration spread of 3%. Furthermore, the increment in the desorbed water vapour rate was only about 173g/h in the 4th test sequence ($\vartheta_{hw} = 89.2°C$) compared to the 3rd test sequence ($\vartheta_{hw} = 79.8°C$) . An explanation of such underestimated value could be that by increasing the heating-water inlet temperature, the air temperature increases as well, the air outlet temperature was $\vartheta_{a,o} = 68.8°C$ for a heating-water inlet temperature of $\vartheta_{hw} = 89.2°C$ compared to $\vartheta_{a,o} = 61.2°C$ for a heating-water inlet temperature of $\vartheta_{hw} = 79.8\,°C$. Referring to the psychrometric chart and considering the ±1% accuracy of the relative humidity sensor, the air

humidity ratio alters exponentially by increasing the air temperature.

6.5 Discussion

The experimental results are in general in line with the expected trends like the increase of the water vapour desorption rate, $\dot{m}_v$, for an increase in the liquid desiccant flow rate in Figure 11 and an increase in the charging temperature in Figure 17. The larger the mass flow rate of the desiccant solution $\dot{m}_{sol}$, the smaller is the mass fraction spread of the desiccant $\Delta\xi$, while the solution temperature rises less. Due to higher mass fractions and lower temperatures of the liquid desiccant on the absorber plate at high desiccant mass flow rates, the water vapor pressure of the solution is reduced.

Only few related studies are available in literature which present investigations of heat and mass exchangers in cross flow configuration in general, and even less for low flow systems. For the developed components presented in the present study the energy storage values C_s of up to 117 kWh/m^3 are significantly increased compared to high flow systems in which the air to solution mass ratio is usually $r_m < 1$ as presented in the literature, for example the system by Fumo and Goswami [35]. The mass fraction spread by Fumo and Goswami was in the range of $\Delta\xi$=0.006 kg/kg and the energy density was in the range $C_s = 8\ kWh/m^3$. The air to solution mass ratios in the present study were in the range $r_m = 5\ to\ 35$ is clearly reflected in higher concentration spreads as well energy densities.

The volumetric energy storage capacity Cs is a decisive measure to reach small storage sizes. However, the experimentally evaluated values of Cs in this study are lower than expected theoretically, presumably as a result of inadequate wetting of the tube bundle. Keßling *et al.* [15] studied experimentally an internally cooled/heated absorber/regenerator. LiCl-H_2O was used as a desiccant solution with extremely low flow rates "micro-flow" of the desiccant solution. For the micro-flow system presented by Keßling the air to desiccant mass ratio was in the range $r_m = 40\ to\ 150$ and he achieved a storage density up to 700 MJ/m^3 (190 kWh/m^3) that represents half of the analytical estimated storage capacity. Keßling attributed the reason for this deviation to a bad wetting of the absorber plates with a wetting factor of 30 %.

In the present study, the most influencing inlet parameter for storage capacity enhancement was the desiccant solution flow rate. The energy storage capacity is inversely proportional to the solution flow rate in such away the lower the solution flow rate is, the higher is the energy storage capacity. In the performed experiments, the storage capacity increased from Cs=36 kWh/m^3 for a solution mass flow rate of m= 82 kg/h, to Cs= 117 kWh/m^3 for m=11 kg/h. Decreasing the desiccant flow rate will increase the exposure time of the desiccant solution and thereby enhance the desired mass and heat transfer, thereby, the solution is concentrated significantly. The great difference in salt concentration of diluted and strong salt solution ($\Delta\xi$) is necessary for a high storage capacity.

7. CONCLUSION

A tube-bundle heat and mass exchanger was designed, constructed and instrumented to evaluate its performance. Previous studies by the authors illustrated the challenges associated with using plastics in environments subject to significant temperature change and show the importance of dealing with the mechanical design aspects (e.g., thermal expansion coefficients and tolerances). To overcome the technical shortcomings of plastics, a unique regenerator design, based on an internally heated coated-copper tube bundle, was developed and evaluated. This design resolved some of the practical design limitations of plastic devices while increasing heat transfer and limiting corrosion. The presented regenerator proved high thermal stability by high water temperatures up to 89.2°C. However, the construction of the tube-bundle device proved challenging, particularly related to issues of desiccant distribution.

Through a series of parametric tests, optimal configuration and operation were identified in terms of: desiccant flow rate, inlet air temperature, inlet desiccant temperature, and inlet heating water temperature. The results indicate that water transfer rate from the diluted solution increases by increasing the desiccant flow rate, desiccant solution inlet temperature, and inlet heating water temperature. A parametric analysis with boxplots indicates that the median of the heating-water inlet temperature is the highest among the four controlled variables regarding the water vapour desorption rate. The heating-water inlet temperature has the highest impact on the water vapour desorption rate, followed by the air to solution mass ratio. Also, the boxplot shows that changing the air inlet temperature has the lowest effect on the water vapour desorption rate for the given operating conditions, as shown in Figure 19. The concentration spread is reduced by increasing the desiccant flow rate. An increment in the solution concentration of 6% is achieved for a solution flow rate of 3 g/s compared to an increment of 1.7% for a solution flow rate of 23 g/s. The box plot indicates that the solution flow rate and the heating water inlet temperature have the highest impact on $\Delta\xi$, as shown in Figure 20.

Further improvements in the regenerator design need to be considered by adjusting the installation of the tube-bundle. The tube-bundle needs to be connected in such a way that minimizes the distance between the adjacent tubes and to minimize the tolerance in the bended tubes. This in turn will enhance the wetting factor of the textile attached over the tubes. Also, a long term monitoring of the applied powder coating layer is necessary as a result of the high corrosive environment which increases by high water temperatures

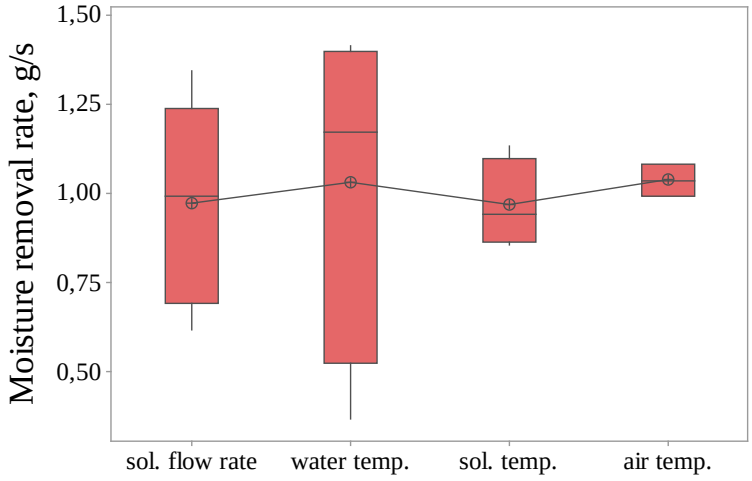

Fig. 19. Box- and whisker plot of the effect of the controlled variables on the water vapour desorption rate.

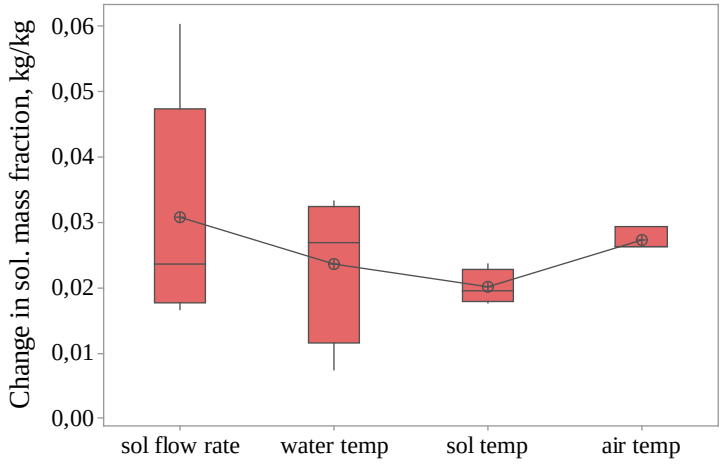

Fig. 20. Box- and whisker plot of the effect of the controlled variables on the concentration spread.

ACKNOWLEDGEMENT

Sincere thanks for the funding by the German Ministry for Research and Education, BMBF, in the framework of the research project "Open Sorption Processes" (OpenSorp, AZ 03SF 0444). Also, the support of Prof. Dr. Ulrike Jordan is gratefully acknowledged.

NOMENCLATURE

A	area	m^2
a	transverse pitch ratio	
α	heat transfer coefficient	$W\,.\,m^{-2}.K^{-1}$
b	longitudinal pitch ratio	
c_p	specific heat capacity	$kJ\,.\,kg^{-1}.K^{-1}$
C_s	storage capacity	$kWh\,.\,m^{-3}$
d	diameter	m
f_A	arrangement factor	
h_{fg}	enthalpy of vaporization	$kJ\,.\,kg^{-1}$
l	length	m
m	mass	kg
$\dot{m}$	mass flow rate	$kg \cdot h^{-1}$
p	pressure	Pa
$\dot{Q}$	heat flow	W
r	radius	m
r_m	air to solution mass flow ratio	
T	thermodynamic temperature	K
U	overall heat transfer coefficient	$W\,.\,m^{-2}.K^{-1}$
X	mass of water per mass of LiCl salt	$kg_{H2O}.kg_{LiCl}^{-1}$
V	volume	m^3
Δ	difference	
λ	thermal conductivity	$W.m^{-1}.K^{-1}$
ω	humidity ratio	$g_w \cdot kg_{d.a}^{-1}$
φ	relative humidity	
ψ	void fraction	
ρ	density	$kg \cdot m^{-3}$
ϑ	temperature	$°C$
ξ	mass fraction of the desiccant	$kg_{LiCl} \cdot kg_{sol}^{-1}$

Subscripts

a	air
con	concentrated
dil	diluted
e	equilibrium
hw	heating water
i	inlet conditions
LiCl	lithium chloride as salt
o	outlet conditions
s	saturated
sol	solution
stag	staggered
ss	solution side
v	water vapour
w	water

REFERENCES

[1] Miller W.M., 1983. Energy storage via desiccants for food/agricultural applications. *Energy in Agriculture* 2: 341–354.

[2] Kabeel A.E., Khalil A., Elsayed S.S., and Alatyar A.M., 2018. Theoretical investigation on energy storage characteristics of a solar liquid desiccant air conditioning system in Egypt. *Energy* 158: 164–180.

[3] Elzahzby A.M., Kabeel A.E., Bassuoni M.M., and Abdelgaied M., 2014. Effect of inter-cooling on the performance and economics of a solar energy assisted hybrid air conditioning system with six stages one-rotor desiccant wheel. *Energy Conversion and Management* 78: 882–896.

[4] Al-Alili A., Hwang Y., and Radermacher R., 2015. Performance of a desiccant wheel cycle utilizing new zeolite material: Experimental investigation. *Energy* 81: 137–145.

[5] Aprea C., Greco A., and Maiorino A., 2015. The application of a desiccant wheel to increase the energetic performances of a transcritical cycle. *Energy Conversion and Management* 89: 222–230.

[6] De Antonellis S., Intini M., Joppolo C.M., Molinaroli L., and Romano F., 2015. Desiccant wheels for air humidification: An experimental and numerical analysis. *Energy Conversion and Management* 106: 355–364.

[7] Hauer A., 2007. *Sorption Theory for Thermal Energy Storage, in Thermal Energy Storage for Sustainable Energy Consumption*, ed H. Paksoy, Springer, Dordrecht, 2007.

[8] Hauer A. 2007. *Adsorption Systems for Thermal Energy Storage - Design and Demonstration Projects, in Thermal Energy Storage for Sustainable Energy Consumption*, ed H. Paksoy, Springer, Dordrecht, 2007.

[9] ASHRAE (1997). *1997 Handbook – Fundamentals.* American Society of Heating, Refrigerating and Air-Conditioning Engineers. Atlanta, Georgia.

[10] Yu N., Wang R.Z., and Wang L.W., 2013. Sorption thermal storage for solar energy. *Progress in Energy and Combustion Science* 39, 489–514.

[11] Lowenstein A., 2008. Review of liquid desiccant technology for HVAC applications. *HVAC&R Research* 14: 819–839.

[12] Al-Farayedhi A.A., Gandhidasan P., and Al-Mutairi M.A., 2002. Evaluation of heat and mass transfer coefficients in a gauze-type structured packing air dehumidifier operating with liquid desiccant. I*nternational Journal of Refrigeration 25*: 330–339.

[13] Longo G.A. and A. Gasparella. 2005. Experimental and theoretical analysis of heat and mass transfer in a packed column dehumidifier/regenerator with liquid desiccant. *International Journal of Heat and Mass Transfer* 48: 5240–5254.

[14] Öberg V. and D.Y. Goswami. 1998. Experimental study of the heat and mass transfer in a packed bed liquid desiccant air dehumidifier. J*ournal of Solar Energy Engineering* 120: 289.

[15] Kessling W., Laevemann E., and Peltzer M., 1998. Energy storage in open cycle liquid desiccant cooling systems. *International Journal of Refrigeration* 21: 150–156.

[16] Lowenstein A., Slayzak S., and Kozubal E., 2006. A zero carryover liquid-desiccant air conditioner for solar applications, in: *Solar Energy*. Presented at the ASME 2006 International Solar Energy Conference, ASME, Denver, Colorado, USA, pp. 397–407.

[17] Bassuoni M.M., 2013. Parametric study of a single cycle two-stage structured packing counter flow air dehumidifier using two feeding desiccant solution lines. *Energy Conversion and Management* 75: 175–183.

[18] Cai D., Qiu C., Zhang J., Liu Y., Liang X., and He G., 2017. Performance analysis of a novel heat pump type air conditioner coupled with a liquid dehumidification/humidification cycle. *Energy Conversion and Management* 148: 1291–1305.

[19] Kim M.-H., Park J.-Y., and Jeong J.-W., 2015. Simplified model for packed-bed tower regenerator in a liquid desiccant system. A*pplied Thermal Engineering* 89: 717–726.

[20] Wang Z., Zhang X., and Li Z., 2017. Investigation on the coupled heat and mass transfer process between extremely high humidity air and liquid desiccant in the counter-flow adiabatic packed tower. *International Journal of Heat and Mass Transfer* 110: 898–907.

[21] Lowenstein A., Slayzak S., Ryan J., Pesaran A., 1998. *Advanced Commercial Liquid-Desiccant Technology Development Study* (No. NREL/TP-550-24688, 12099).

[22] Cheng Q. and X. Zhang. 2013. Review of solar regeneration methods for liquid desiccant air-conditioning system. *Energy and Buildings* 67, 426–433.

[23] Naik B.K., Soni A., Kumar A., Muthukumar P., and Somayaji C., 2016. Coupled heat and mass transfer analysis of an adiabatic dehumidifier – unique approach. *Energy Procedia* 90: 305–315.

[24] Naik B.K., Muthukumar P., and Sunil Kumar P., 2018. A novel finite difference model coupled with recursive algorithm for analyzing heat and mass transfer processes in a cross flow dehumidifier/regenerator. *International Journal of Thermal Sciences* 131: 1–13.

[25] Naik B.K. and P. Muthukumar. 2019. Experimental investigation and parametric studies on structured packing chamber based liquid desiccant dehumidification and regeneration systems. *Building and Environment* 149: 330–348.

[26] Hublitz A., 2008. Efficient Energy Storage in Liquid Desiccant Cooling Systems. A *Ph.D. Thesis*, Technische Universitaet Muenchen, Muenchen, Germany.

[27] Gommed K. and G. Grossman. 2007. Experimental investigation of a liquid desiccant system for solar cooling and dehumidification. *Solar Energy* 81: 131–138.

[28] Abdel-Salam A.H., McNevin C., Crofoot L., Harrison S.J., and Simonson C.J., 2016. a field study of a low-flow internally cooled/heated liquid desiccant air conditioning system: quasi-steady and transient performance. *Journal of Solar Energy Engineering* 138: 031009.

[29] Jaradat M., Fleig D., Vajen K., and Jordan U., 2018. Investigations of a dehumidifier in a solar-assisted liquid desiccant demonstration plant. *Journal of Solar Energy Engineering* 141: 031001.

[30] Brinson H.F. and L.C. Brinson. 2008. *Polymer Engineering Science and Viscoelasticity: An Introduction*. Springer.

[31] Mesquita L., 2007. Analysis of a flat-plate liquid-desiccant dehumidifier and regenerator. A *PhD Thesis*, Queen's University, Kingston, Canada.

[32] Yamaguchi S., Jeong J., Saito K., Miyauchi H., and Harada M., 2011. Hybrid liquid desiccant air-conditioning system: Experiments and simulations. *Applied Thermal Engineering* 31: 3741–3747.

[33] VDI Heat Atlas, 2013. 11th Edition Berlin, Heidelberg: Springer Vieweg Verlag.

[34] Conde M.R., 2004. Properties of aqueous solutions of lithium and calcium chlorides: formulations for use in air conditioning equipment design. *International Journal of Thermal Sciences* 43: 367–382.

[35] Fumo N. and Goswami. 2002. Study of an aqueous lithium chloride desiccant system: air dehumidification and desiccant regeneration. *Solar Energy* 72: 351–361.